Exposure accumulation drives age-dependent disease architectures and polygenic risk scores

Xilin Jiang[1,2,3,4,5,*], Alkes L. Price[3,4,6], John Danesh[1,2,7,8,9,10], Gil McVean[11], Michael Inouye[1,2,7,9,12,13], Sarah Urbut[4,14], Arun Durvasula[15,16,17,*]

1. British Heart Foundation Cardiovascular Epidemiology Unit, Department of Public Health and Primary Care, University of Cambridge, Cambridge UK
2. Victor Phillip Dahdaleh Heart and Lung Research Institute University of Cambridge, Cambridge UK
3. Department of Epidemiology, Harvard T.H. Chan School of Public Health Boston MA USA
4. Broad Institute, Cambridge, MA USA
5. Cambridge Centre for AI in Medicine, University of Cambridge, Cambridge UK
6. Department of Biostatistics, Harvard T.H. Chan School of Public Health Boston MA USA
7. British Heart Foundation Centre of Research Excellence, University of Cambridge, Cambridge, UK
8. National Institute for Health and Care Research Blood and Transplant Research Unit in Donor Health and Behaviour, University of Cambridge, Cambridge, UK
9. Health Data Research UK Cambridge, Wellcome Genome Campus and University of Cambridge, Cambridge, UK
10. Department of Human Genetics, Wellcome Sanger Institute, Hinxton, UK
11. Ellison Institute of Technology, Oxford, UK
12. Cambridge Baker Systems Genomics Initiative, Department of Public Health and Primary Care, University of Cambridge, Cambridge, UK
13. Cambridge Baker Systems Genomics Initiative, Baker Heart and Diabetes Institute, Melbourne, Victoria, Australia
14. Cardiology Division, Massachusetts General Hospital, Boston, MA USA.
15. Division of Epidemiology, Department of Population and Public Health Sciences, Keck School of Medicine, University of Southern California, Los Angeles, CA
16. Center for Genetic Epidemiology, Department of Population and Public Health Sciences, Keck School of Medicine, University of Southern California, Los Angeles, CA
17. Department of Quantitative and Computational Biology, University of Southern California, Los Angeles, California, USA

* Correspondence: xj262@medschl.cam.ac.uk (XJ); arun.durvasula@med.usc.edu (AD)

Abstract

Our understanding of the dependence of the genetic and environmental architecture of common diseases on age is incomplete. Here, we use longitudinal data to separate age-dependent genetic and environmental variance across complex traits and diseases. When applying our approach to 16 UK Biobank quantitative traits (average *N*=180K), we found environmental variance accumulates with age, leading to decreasing heritability with age, which follows an exposure accumulation model that is distinct from gene-age interaction model. Heritability decreases with age for 5 traits including systolic blood pressure and lung function (FEV1/FVC), with an average change of −17.8% with age per 10-years. We demonstrated that majority of the decreasing heritability comes from exposure accumulation, instead of gene-age interaction, using longitudinal phenotypic correlations. For diseases, environmental variance in disease liability also accumulates with age for 5 of 9 diseases, with an average decrease in heritability of −18.1% per 10 years. A liability-threshold model with exposure accumulation explains 86% of decreasing PRS prediction R^2 with age in 9 UK Biobank complex diseases. Finally, we show that both genetic and non-genetic predictors have decreasing prediction accuracy with age in 61 predictor-disease pairs. Taken together, our results demonstrate that the age-dependent liability-threshold model with exposure accumulation is a general disease model, suggesting ascertaining younger cohorts is more powerful for training both genetic and non-genetic risk prediction models.

Introduction

The extent to which genetics and environmental exposures interact with age when contributing to phenotypic variation in a population is unclear[1,2]. Previous studies have found evidence that environmental exposures can account for more phenotypic variation in older individuals, potentially due to the accumulation of exposures as people age[3–5]. However, measuring the relevant environmental exposures throughout an individual's lifetime remains a significant challenge. On the other hand, gene-age interaction, which can arise from multiple sources[6], including proportional amplification of genetic variance[7] and different age profiles of genetic effects across genotypes[8], could drive age-dependent phenotypic variation. Jointly studying the age profiles of genetic and non-genetic components of complex traits can elucidate the architectures of age-dependent complex traits.

Recent work has shown age-varying prediction accuracy for polygenic risk scores (PRS), but whether this observation is driven by gene-age interactions or other mechanisms is unknown[8–14]. Significant challenges remain in studying age-dependent disease architectures. First, disease liability is not observed and performing gene-age interaction tests on binary disease observations may not be informative of interactions on the liability scale[15]. Second, although methods exist for reducing bias in modeling time-to-event data due to censoring, these methods often have assumptions that are not met in empirical data[8].

Here, we estimated the age-dependent profiles of genetic and environment components of complex traits and disease liability. We show that the impact of environmental exposures accumulates with age for a wide range of complex traits and diseases, which causes a decrease in heritability with age. We show that exposure accumulation, under a liability-threshold model[16,17], explains decreasing prediction accuracy of PRS prediction accuracy for 9 diseases in UK Biobank. Finally, we show by simulation and analytical derivation that a liability-threshold model predicts that both genetic and environmental factors will have decreased prediction accuracy for older cases, which we validate in empirical data using 61 predictor-disease pairs.

Results

Overview of methods

We study age-dependent trait architecture under an exposure accumulation (EA) model where liability is linear in genetic, environment, and age quintiles[18], with environmental variance accumulating with age.

The EA model can be formalized under the following:

$$L = G + E + age + \sum_{a=0}^{age} E_a, \quad (1)$$

where L denotes liability, G is the genetic component of liability, E is the environmental component, age is the quintile of age, and E_a is the contribution of age to liability. $\sum_{a=0}^{age} E_a$ is the term arising from the EA model. We study architecture across age quintiles to relax statistical assumptions on the relationship between age and L. We evaluate evidence for 4 additional models that can cause an age-dependent architecture: proportional amplification[7,15] (ref), age-dependent G, exposure accumulation with decay, and non-proportional amplification (**Supplementary Table 1**).

We evaluate evidence of the EA model by estimating age-varying heritability ($\Delta h^2 = h^2_{older} - h^2_{younger}$), which is negative under the EA model. We estimate Δh^2 by estimating the heritability for each age quintile with BOLT-REML[19] and fitting a model where heritability changes linearly with age. We estimate heritability with age and sex as covariates to account for within age quintile variation due to age and sex. We test for non-zero Δh^2 with a likelihood ratio test between the model with age term and a null model where heritability is constant with age. We also evaluate the environmental correlation between age quintiles ($\rho(E_{younger}, E_{older})$), which is expected to be less than 1.0 under the EA model. We use phenotypic correlations (ρ_l), which is an upper bound of $\rho(E_{younger}, E_{older})$ under the EA model, to evaluate evidence of $\rho(E_{younger}, E_{older}) < 1$. We account for error-in-measurement of ρ_l by computing the denoised phenotypic correlation ($\tilde{\rho}_l$) for individuals with three phenotype measurements at different age points. We estimated $\tilde{\rho}_l$ as the ratio of first-third visit ρ_l and first-second visit ρ_l. The ratio cancels the impact of measurement error. We divide $log(\tilde{\rho}_l)$ by the average age difference between the second and third visits to estimate $\tilde{\rho}_l$ between individuals with one year of age difference (see **Methods**).

We estimated Δh^2 and $\tilde{\rho}_l$ for 16 quantitative traits across 180K individuals in the UK Biobank (**Supplementary Table 2**); the sample size reflects a restriction to individuals of British ancestry with diagnostic records from both primary care data and hospital inpatient data, which we imposed to mitigate the impact of missing diagnoses. The quantitative traits in this study were selected following ref. [20] (**Methods**). We use *cross-sectional design* to estimate Δh^2, where we compare individuals with different ages at the baseline visit. We evaluate the impact of recruitment bias that can arise from a cross-sectional design in a secondary analysis. We use *longitudinal measurement* to estimate $\tilde{\rho}_l$, where we compare multiple measurements at different age points of the same individual.

We estimate Δh^2 for the estimated disease liability of 9 diseases (**Supplementary Table 3**). We use 36 quantitative traits (**Supplementary Table 4**) to estimate disease liability at baseline age by predicting binary disease phenotypes from the quantitative traits. We do not estimate $\widetilde{\rho_l}$ for estimated disease liability because we do not have longitudinal measurements for all quantitative traits that were used to estimate disease liability.

We study the impact of age-dependent disease architecture on disease prediction using simulations. We extract age-at-diagnosis for each patient using the first diagnosis in either primary care data or hospital inpatient data to evaluate age-dependent disease prediction accuracy in empirical data. We construct PRS and non-genetic predictors using five-fold cross validation without age stratification. We have publicly released summary data of age-specific heritability, phenotypic correlation, and genetic correlation estimates (see **Data Availability**). We have also released software to compute age-dependent heritability and prediction accuracy (and **Code Availability**).

Age-dependent genetic architecture of quantitative traits

We estimated Δh^2 w.r.t. age of 16 quantitative traits (**Supplementary Table 2**) to evaluate the evidence supporting the EA model. First, we found 5 of the 16 traits have significantly decreasing heritability with age (p<0.05/9, FEV1/FVC, LDL cholesterol, total cholesterol, diastolic blood pressure, and systolic blood pressure) with an average 10-year decrease of 17.8% in h^2 (**Figure 1A**, **Supplementary Table 5, Supplementary Figure 1**). Second, we computed genetic and environmental variance of each age quintile using heritability and phenotypic variance estimates (**Figure 1B, Supplementary Figure 2, Supplementary Figure 3, Supplementary Table 6, Supplementary Table 7**). We estimated phenotypic variance for males and females separately to account for sex differences[7,15], which provides estimates for 32 trait-sex pairs. We found $\Delta var(E)$ is significantly larger than $\Delta var(G)$ for 10 trait-sex pairs (red dots in **Figure 1B**), supporting the EA model. We found $var(E)$ and $var(G)$ vary proportionally with age in traits that do not have significant age-varying heritability (grey dots in **Figure 1B**), supporting a proportional amplification model that has been observed in GxE studies[7,15]. The EA model will move traits above the diagonal line in **Figure 1B**, while the proportional amplification model will move traits along the diagonal line. Taken together, we conclude that FEV1/FVC, LDL cholesterol, total cholesterol, systolic blood pressure, and diastolic blood pressure show evidence for the EA model.

Next, we estimated genetic and phenotypic correlations between age groups to evaluate additional evidence in support of the EA model. $\rho(G_{younger}, G_{older})$ is expected to equal 1.0 and $\rho(E_{younger}, E_{older})$ is expected to be less than 1.0 under the EA model. We found the genetic correlation, $\rho(G_{younger}, G_{older})$, was close to 1.0 for most traits, with exceptions of HbA1c (p=1e-4) and glucose (p=3e-4) (**Figure 2A, Supplementary Table 8**). A genetic correlation less

than 1.0 supports a model where genetic components have different age profiles (**Supplementary Table 1**), which is consistent with our previous work that showed that genetic variants have distinct age profiles in conveying common disease risk[4]. We computed the denoised phenotypic correlation $\widetilde{\rho_l}$ to evaluate the environmental correlation across age ($\rho(E_{younger}, E_{older})$) (**Methods**). For the 11 traits that have longitudinal data for 3 visits, 7 have $\widetilde{\rho_l}$ significantly less than 1.0 (**Figure 2B, Supplementary Table 9**), supporting the EA model. $\widetilde{\rho_l}$ has high correlation with Δh^2 w.r.t. age (ρ=0.61 across 11 traits, **Figure 2C**), which is consistent with the EA model. Specifically, the 3 traits (Systolic BP, Diastolic BP, and FEV1/FVC) that show evidence supporting the EA model in **Figure 1** have the largest difference between $\widetilde{\rho_l}$ and 1. Our analysis of the genetic and environmental correlation between young and old individuals provides orthogonal evidence in support of EA for systolic blood pressure, diastolic blood pressure, and FEV1/FVC.

We performed six secondary analyses to test the robustness of our results. First, we tested whether age-dependent recruitment bias of individuals with different health status could explain decreasing heritability estimates. We created two age-matched samples (mean age: 55.9 vs. 56.6) with high and low numbers of prevalent disease diagnoses (mean diagnoses: 6.8 vs 34.6) and estimated the heritability of 16 quantitative traits in the two groups. We observed minimal heritability differences between the two groups, which suggests that biased recruitment of healthier older individuals in the UK Biobank[21] does not contribute to the decreasing heritability estimates with age (**Supplementary Figure 4**). Second, we evaluated the amplification models[7] by estimating changes in genetic variance w.r.t. age for 32 trait-sex pairs (**Supplementary Figure 2, Supplementary Table 7**). We found 25 traits with age-varying genetic variance, align with previous GxSex and GxE studies that report amplifications[7,15]. Third, we tested an alternative model where exposure accumulation decays with age by identifying traits with Δh^2 close to zero but a denoised phenotypic correlation less than 1.0 across age bins. We found evidence support this model for BMI and body WHR among the traits that we can estimate $\widetilde{\rho_l}$ (i.e. those with multiple measurements) (**Supplementary Table 9**). Fourth, we tested a non-proportional amplification model by identifying traits with both genetic correlation and denoised phenotypic correlation close to 1 but age-varying heritability (**Supplementary Table 9**). We found no such traits among the traits that we can estimate $\widetilde{\rho_l}$. Fifth, we estimated genetic correlation between the top and bottom age quantiles (median age difference = 22.0) without meta-analyzing across age bins and found smaller $\rho\left(G_{young}, G_{old}\right)$ compared with the meta-analyzed results with larger standard errors (**Supplementary Figure 5**). Sixth, we tested whether using age in years instead of age quintiles can explain more variance in quantitative traits. We found age quintiles explains similar R^2 as age in years (**Supplementary Figure 6A**), suggesting age quintiles capture the majority of age-related variation while allowing us to use standard methods to compute heritability and genetic correlations. We found adding an additional age^2 covariate to the age in years explains more quantitative trait variance (mean R^2= 0.024 across 16 traits) than the model with only linear age in years (mean R^2= 0.022 across 16 traits).

Taken together, these results support exposure accumulation as the primary driver of age-dependent architecture in quantitative traits.

Age-dependent genetic architecture of estimated disease liability

We next investigated whether the liability of 9 diseases (**Supplementary Table 3**) is consistent with the EA model. We estimated disease liability by applying LASSO[22] to 36 quantitative traits (**Supplementary Table 4**) measured at baseline and predicting disease status in the entire population (i.e. across all age bins). We use the value predicted by LASSO as estimated liability to approximate disease liability (**Methods**).

We hypothesized that estimated liability is highly correlated with the true disease liability at the baseline age, thus can be used to study the age-dependent architecture of disease liability. We confirmed that the estimated liability achieves high accuracy across nine diseases, with an average liability-scale correlation of 0.603 (s.d. = 0.206 across nine diseases, **Supplementary Table 10**) with case-control status. We applied the same methods as in the quantitative trait analysis to the estimated liabilities to estimate Δh^2 and $\rho(G_{younger}, G_{older})$. We validated that h^2 of estimated liability is similar to the liability-scale h^2 of the respective diseases (**Supplementary Figure 7**). We found the heritability of the predicted liability significantly decreases for 5 of the 9 predicted disease liabilities (**Figure 3A**, **Supplementary Table 11**, mean Δh^2 = -18.1%±2.7% for every 10 years of age), which supports the EA model of disease liability. We observe genetic correlations across age bins ($\rho(G_{younger}, G_{older})$) are significantly different from 1 for coronary artery disease (CAD) and T2D (**Figure 3B**, **Supplementary Table 12**), which aligns with previous observations of heterogeneous age profiles in CAD[8] and subtypes of T2D[23–25]. Taken together, we determined the estimated liabilities of asthma, hypertension, high lipid, COPD, and high cholesterol follow the EA model.

Simulations implicate factors contributing to age-dependent disease PRS accuracy

We hypothesized that the following 3 factors could contribute to age-dependent disease PRS accuracy: (i) age-dependent liability under a liability threshold model[8,16]; (ii) prediction of incident cases (instead of prevalent cases)[26]; and (iii) exposure accumulation under our new EA model. We refer to these three hypotheses as factors (i) - (iii).

First, the intuition of factor (i) is that older cases have disease liability closer to healthy individuals compared to younger cases (see **Methods** and **Supplementary Note**). Under the liability-threshold model (**equation 1**), L increases as the population ages, which causes older cases to have liability that is closer to the healthy controls compared to the cases that reached the threshold at a younger age (**Figure 4A**, ref [18]). Therefore, the difference between cases and

controls becomes smaller for the older population, which causes decreasing prediction accuracy. In **Supplementary Note**, we show that the difference between the genetic values of cases and controls strictly decreases with age, which aligns with the intuition that liability of older cases is closer to healthy controls.

Second, the intuition of factor (ii) is that excluding prevalent cases at baseline will create negative correlation between the predictable component and non-predictable component of disease liability, which reduces prediction accuracy (see **Supplementary Note)**. We note that there are two ways to define cases and controls at a specific age point (**Figure 4A**). First, *prevalent case association* defines cases as individuals who are diagnosed with the disease before the age point and controls as individuals who have not had a diagnosis of the disease at least until the age point; prevalent case association is a common choice in constructing genetic risk scores[20,27–30]. Second, *incident case prediction* defines cases as individuals who are diagnosed for the first time within a time window after the age point and controls as individuals who are not diagnosed at least until the end of the time window; incident case prediction is a common choice in clinical risk prediction[31,32]. We report results from both case-control definitions but focus on the latter because incident case prediction has more clinical utility.

Third, the intuition of factor (iii) is that PRS prediction accuracy decreases with age when heritability decreases with age (see **Supplementary Note**). Under the proposed EA model, heritability will decrease due to exposure accumulation, causing decreasing PRS accuracy with age.

We performed simulations to evaluate the contribution of factors (i)-(iii) to age-dependent prediction accuracy. Our simulation framework modeled liability increasing linearly with age. The age of onset is determined when the liability of an individual reaches a fixed threshold. We evaluate prediction accuracy using the observed R^2 with 1:1 case-control ratio (${R^2}_{obs}$), area under the ROC Curve (AUC), liability-scale R^2 (${R^2}_{liab}$), and log odds ratio ($logOR$). Further details are provided in the **Methods** section.

${R^2}_{obs}$, AUC, and $logOR$ all decrease with age for both prevalent case association and incident case prediction, while ${R^2}_{liab}$ decreases with age for incident case prediction but not for prevalent case association, supporting the contribution of factor (i) to age-dependent prediction accuracy (orange and purple curves in **Figure 4B; Supplementary Figure 8A**). Incident case prediction accuracy decreases more than the prevalent case association accuracy, supporting the contribution of factor (ii). We found that prediction accuracy under the EA model decreases more than under linear liability-threshold model, supporting the contribution of factor (iii) (grey curves in **Figure 4B)**. We estimated ${R^2}_{liab}$ under a normal distribution assumption[33] in empirical data analyses. We evaluated the accuracy of this approximation using simulations and found it was accurate (**Supplementary Figure 8B**).

We show in the **Supplementary Note** that the *relative* contribution of factor (i) to age-dependent prediction accuracy depends on the R^2_{liab} of the predictor to the underlying L. To validate this hypothesis, we simulated predictors with varying R^2_{liab} to the underlying L, representing a perfect predictor ($R^2_{liab} = 99\%$), a strong predictor ($R^2_{liab} = 50\%$), a clinical score ($R^2_{liab} = 20\%$), and a PRS ($R^2_{liab} = 5\%$). Prediction accuracy decreased more steeply with age for weaker predictors, while the difference is negligible between the clinical risk score and PRS (**Figure 4C, Supplementary Figure 8A**).

Our analyses show that prediction accuracy decreases with age under the liability-threshold model (factor (i)) using both analytical results and simulations, while the decreasing slope is steeper when predicting incident cases (factor (ii)), predicting phenotypes that follow the EA model (factor (iii)), and the predictors have low overall R^2_{liab}.

Age-dependent prediction accuracy of PRS is partially consistent with liability-threshold model and prediction of incident diseases

We next evaluated whether the age-dependent disease PRS accuracy is consistent with factor (i) and (ii) in empirical data. We computed PRS using BOLT-REML with fivefold cross validation for 9 diseases without age stratification. We divided the cases into age quintiles based on the earliest diagnosis age of each patient and created sample sets with a 1:1 case-control ratio to ensure each age bin has the same sample size and case-control ratio. We computed 4 metrics to measure incident case prediction accuracy: log hazard ratio ($logHR$), log odds ratio ($logOR$), the effect size of PRS in a linear regression on case-control status, and R^2_{obs}. We also compute R^2_{obs} for prevalent case association using the median age of each age quintile as the age index. We report the change of the 4 metrics ($logHR$, $logOR$, linear regression effects, and R^2_{obs}) by fitting a model where the metric changes linearly with age. Briefly, we test for non-zero changes in each metric with a likelihood ratio test between the model with age term and a null model where the metric is constant with age (**Methods**). We report the 10-year change of each metric relative to the estimates in the entire population.

We found PRS accuracy decreases with age across all diseases we studied, consistent with factor (i). We started by evaluating the $logHR$ of each PRS to account for censoring. We found that the $logHR$ of each PRS significantly decreased with age for 6 of the 9 diseases ($p<0.05/9$, **Figure 5A**, **Supplementary Table 10**), which aligns with a previous study that used lead GWAS associations and observed decreasing effect sizes with age[8]. On average, the $logHR$ of each PRS in the oldest quintile was 51%±5% of the youngest quintile. For example, the $logHR$ of the PRS for predicting hypertension was 0.39±0.01 for the youngest quintile of cases (median(age_{onset}) = 47.1) and 0.16±0.01 for the oldest quintile of cases (median(age_{onset}) = 72.2). The $logHR$ of the PRS for predicting T2D is 0.32±0.02 for the youngest quintile of cases (median(age_{onset}) = 47.7)

333 and 0.22±0.02 for the oldest quintile of cases (median(age_{onset}) = 72.8). These observations were
334 consistent across different prediction accuracy metrics of PRS ($R^2{}_{obs}$, $logOR$, and linear
335 regression effects, **Supplementary Figure 9, Supplementary Figure 10,** and **Supplementary**
336 **Table 13**). We focus on $R^2{}_{obs}$ in later sections because it is on the same scale as h^2. We found
337 the average 10-year decrease for incident case prediction accuracy ($R^2{}_{obs}$) was greater than the
338 10-year decrease in accuracy for prevalent case association (**Figure 5B, Supplementary Table**
339 **14**), consistent with simulations of factor (ii) in **Figure 4B** (orange curves versus purple curves,
340 respectively). For example, $R^2{}_{obs}$ for PRS predicting hypertension decreases 50.0%±1.7% every
341 10 years of age in incident case prediction and 26.8%±3.3% for prevalent case association. $R^2{}_{obs}$
342 for PRS predicting T2D decreases 25.1%±4.2% every 10 years of age in incident case prediction
343 and no longer decreases for prevalent case association (slope= -2.9%±4.2% per 10 years). Our
344 analyses indicate that PRS prediction accuracy generally decreases significantly with age.
345
346 *Exposure accumulation substantially impacts age-dependent disease PRS accuracy*
347
348 We next evaluated whether the liability-threshold model (factor (i)), for incident case prediction
349 (factor (ii)), and the EA model (factor (iii)) can explain age-dependent disease PRS accuracy in
350 empirical data. We focus on incident case prediction so that all reported age-dependent
351 prediction accuracy contains the contribution of factor (ii). We create quantitative risk scores
352 (QRS) using quantitative traits to predict diseases. Because quantitative traits contain both
353 genetic and non-genetic information, QRS does not contain the impact of the EA model.
354 Therefore, age-dependent QRS prediction accuracy represents the contribution from factor (i)
355 and factor (ii). We used the same 36 baseline quantitative traits to create QRS for each disease
356 and add Gaussian noise so that QRS and PRS have the same $R^2{}_{liab}$ in the entire population
357 (**Methods**). We compute the proportion of observed decrease in PRS accuracy with age that can
358 be explained by each model to evaluate the contribution of the factor (i)-(iii) (**Methods**).
359
360 We found the liability-threshold model (factor (i)) and EA models (factor (iii)) together explain
361 the observed age-dependent prediction accuracy of PRS for incident case prediction (factor (ii)).
362 First, under the liability-threshold model for incident case prediction (factor (i)+(ii)), predictors
363 using genetic data and predictors using non-genetic data (*i.e.* measurements of quantitative traits
364 and environmental exposures) are expected to have the same age-dependent prediction accuracy,
365 if they explain the same amount of variance in the liability ($R^2{}_{liab}$) (**Figure 4C**). We used the
366 change of QRS $R^2{}_{obs}$ with age to estimate the contribution from factor (i) + (ii) (**Methods**). We
367 found 65.1%±11.3% of the change of PRS $R^2{}_{obs}$ with age are explained by these two factors
368 (**Figure 6A**, **Supplementary Table 15** and **Supplementary Table 16**). The change of QRS
369 $R^2{}_{obs}$ with age is significantly different from the change of PRS $R^2{}_{obs}$ with age for hypertension
370 (p=6e-8), asthma (p = 9e-13), and CAD (p = 7e-7). We determined that factor (i) + (ii) explains
371 most, but not all of the decreasing PRS prediction accuracy. Second, under the EA model (factor
372 (iii)), the heritability of disease liability decreases with age, which causes PRS (which only

373 captures genetic variance) accuracy to decrease with age. We found Δh^2 of disease liability is not
374 large enough to fully explain the decrease in PRS prediction accuracy (**Figure 6B**), suggesting
375 the EA model in disease liability (factor (ii)) is insufficient to explain all of decreasing PRS
376 prediction accuracy.
377
378 Lastly, we combine the effect of EA model with liability-threshold model by computing the
379 product of QRS ${R^2}_{obs}$ and h^2 of predicted liability as the expected prediction accuracy of PRS,
380 which captures the contribution of factors (i), (ii), and (iii). We determined that 85.8%±9.8% of
381 the observed age profiles of PRS is explained by the factor (i)+(ii)+(iii) (**Figure 6C,**
382 **Supplementary Table 17**). A model with factors (i)+(ii)+(iii) explains significantly more
383 observed $\Delta {R^2}_{obs}(PRS)$ with age than the model without factor (iii) (p = 4e-6). We note that
384 CAD cannot be explained by our models (p = 3e-7 for x and y difference in **Figure 6C**). CAD
385 also has $\rho(G_{younger}, G_{older})$ < 1.0 (**Figure 3B**), suggesting that age-dependent genetic
386 heterogeneity might cause the deviation from the liability-threshold + EA model. Taken together,
387 our results suggest that the liability-threshold (factor (i)), incident case prediction (factor(ii)), and
388 the EA model (factor (iii)) explain age-dependent prediction accuracy of PRS.
389
390 *Age-dependent accuracy of non-genetic predictors of disease*
391
392 We investigated whether the liability-threshold model applies to age-dependent accuracy of both
393 genetic and non-genetic predictors. We constructed risk predictors using the 36 quantitative
394 measurements as non-genetic variables to further validate the liability-threshold model as a
395 general model of disease. We note these 36 quantitative measurements contain both genetic and
396 non-genetic (but predominantly non-genetic), but we use "non-genetic" to distinguish from
397 analysis that focus on G. For each disease, we constructed 4 predictors with varying prediction
398 power: (1) "QRS" predictor which is a LASSO predictor that uses all 36 quantitative
399 measurements, (2) A "Top 3" predictor that is a joint linear predictor trained using the top three
400 variables ranked by the ${R^2}_{liab}$ with target disease, (3) "single (strong)" predictors which are the
401 quantitative measurements that rank 1st-3rd by the ${R^2}_{liab}$ with target disease, (4) "single
402 (weak)" predictors which are the quantitative measurements that rank 4th and 5th. We trained all
403 predictors using five-fold cross validation and estimated their prediction accuracy of diseases in
404 each age quintile based on baseline UK Biobank visit. We then computed the change of ${R^2}_{obs}$
405 w.r.t. age for each predictor using the same method as the previous sections.
406
407 Predictors with greater prediction power in the entire population have less age-dependent
408 prediction accuracy (**Figure 7A**, **Supplementary Table 18,** and **Supplementary Table 19**), as
409 predicted by simulation results (**Figure 4C, Supplementary Note**). Relative change of R^2_{obs}
410 w.r.t. age is -47.6%±1.3% for "single (weak)" predictors (avg(${R^2}_{liab}$) = 9.8%) and -23.6%±1.1%
411 for "QRS" predictors (avg(${R^2}_{liab}$) = 32.3%), averaging across the 9 diseases. We further expand
412 to 10 predictors for each disease (QRS, "Top 3", each of the top 5 predictors, "top 2", PRS, PRS

+ QRS, restricting to predictors with $R^2{}_{liab}$ > 5% for adequate power) and found strong positive correlations between relative change of R^2_{obs} w.r.t. age and $R^2{}_{liab}$ across disease-predictor pairs (**Figure 7B**, slope = 0.64, p =1.2e-5). We conclude that predictors that use environment variables have decreasing accuracy with age and the effect is stronger for predictors with low overall prediction accuracy, suggesting combining genetic and non-genetic predictors can increase prediction power in older populations.

Discussion

We systematically quantified age-profiles of genetic and environmental variation to understand how complex disease architecture and polygenic risk score (PRS) accuracy vary with age. We found exposure accumulation is common in quantitative traits and complex diseases. We found the age-dependent PRS accuracy can be explained by a combination of a liability-threshold model and the exposure accumulation model. Our analysis was enabled by a novel approach to study estimated disease liability. Finally, we found both genetic and non-genetic predictors decrease in prediction accuracy with age in empirical data and simulations.

Our study represents an advance over previous studies that investigate age-dependent effects. First, we identify changes in genetic and environmental variance across 16 complex quantitative traits and 9 diseases. While previous work has studied age-dependent effects, they have focused on single variant effects[5] or have studied a limited set of phenotypes[4]. Second, to the best of our knowledge, our work is the first to quantify how environmental variance in complex traits accumulates with age using longitudinal data. Third, our work is the first to provide a quantitative explanation for the decrease in prediction accuracy for genetic and non-genetic predictors. While other studies have observed this phenomenon, they have not been able to explain it[8,13]. We note, however, that CAD was an exception to the EA model and, while we speculate that this may be due to age-dependent genetic heterogeneity, this is something of a mystery to be resolved in subsequent studies. Lastly, our work demonstrates that PRS trained and tested using prevalent case association[20,27–30] shows different age-dependent accuracy compared with incident case prediction, underscoring the importance of evaluating PRS accuracy using incident case prediction, which has greater clinical utility[34–37].

Our study has several implications. First, the EA model suggest GWAS study can increase power by accounting for age-dependent heritability. In particular, we hypothesize that mixed effect model can increase power by modelling age-specific random effects. Second, the EA model suggests when incorporating PRS in clinical risk models, PRS should be weighted differently with age to increase power. Third, our results suggest all predictors (*i.e.* genetic or non-genetic) of disease have age-dependent accuracy, while predictors with stronger prediction power in the entire population will have more robust prediction accuracy at older age. This motivates constructing predictors that combine multiple data modalities to achieve maximal prediction

accuracy across age. Fourth, the observed exposure accumulation suggests genetic effects contribute more to phenotypic variation at early ages, suggesting ascertaining environment variables is critical to accurately predict phenotypes at later ages. Lastly, our results suggest recruiting younger cases can improve power for discovering both genetic and environment biomarkers for diseases. All of these implications motivate directions for future research.

Our study has several limitations. First, our modeling is not able to detect uniformly decreasing genetic variance which can cause decreasing h^2 with age and $\rho\left(G_{young}, G_{old}\right)$ close to 1. However, we believe this is not likely because we found evidence of accumulating environmental variance in the $\widetilde{\rho_l}$ analyses which explains the decreasing h^2 (**Figure 2C**). Second, the age range of our study sample is restricted, with baseline visit age between 40 to 79 years of age. Future analyses with a wider age distribution may discover stronger effects. Third, we use a cross-sectional analysis, which is susceptible to recruitment bias. We tested whether age-dependent recruitment bias of healthier individuals could explain decreasing heritability estimates with age and observed minimal heritability differences between the two groups, suggesting a minimal effect of biased recruitment. Fourth, our analyses uses only individuals of European individuals. While it is of interest to perform the analysis on individuals of other ancestries, currently available data of other genetic ancestry might not have sufficient power for age-stratified analyses. Fifth, our analyses use the UK Biobank data set. It is of interest to replicate the analysis in other cohorts such as All of Us[38]. Sixth, majority of our findings rely on the validity of liability-threshold model, although liability-threshold model has been widely accepted and used[16,17,39–45]. Despite these limitations, our work identifies exposure accumulation as a key aspect age-dependent disease architecture, and our results explain the decreasing genetic and non-genetic disease prediction accuracy with age.

Methods

Study population in UK Biobank

We used the disease diagnosis information from 180,026 individuals whose primary care data (General Practice, GP) was available and of British Isle ancestry. The primary care data are coded in readv2 which were mapped to SNOMED CT (https://digital.nhs.uk/services/terminology-and-classifications/read-codes), SNOMED CT codes were then mapped to ICD-10 codes (using NHS digital's code mapping https://digital.nhs.uk/), which were combined with ICD-10 codes from Hospital Episode Statistics (HES) and mapped to PheCodes [46]. We extracted the earliest diagnosis age using the earliest records from the combined primary care and HES data, which are used as age labels in our analysis. The choice of focusing on individuals with both primary data and HES data was to get the best age at diagnosis for each disease. When combining GP and HES data to extract diagnosis, correlation between binary and quantitative traits increased compared to only using HES data to extract disease (**Supplementary Figure 11**), suggesting that combining GP and HES data capture diagnoses more accurately as correlation decreases when variables are measured with noise.

493
494 Selection of quantitative and binary traits
495 We extracted 36 quantitative traits measured at baseline visit of UK Biobank based on ref. [20]. As
496 our goal is to study disease liability, we selected 9 diseases using phecodes that have
497 interpretable underlying quantitative traits from the 36 quantitative traits (e.g. Hb1Ac for T2D,
498 BMI for obesity, LDLc for hypercholesterolemia) and prevalence higher than 5%
499 (**Supplementary Table 3**). Disease status and age-at-diagnosis were extracted from GP+HES
500 data described in the previous section.
501
502 We corrected blood biochemistry measurement for cholesterol, hypertensive, and diabetic
503 medications: cholesterol (+1 s.d.), LDL-c (+ 1 s.d.), and triglyceride levels (+0.5 s.d.) were
504 corrected for lipid lowering medication[47]; systolic blood pressure (+15 mm Hg) and diastolic
505 blood pressure (+ 10 mm Hg) were corrected for hypertension medication[48]; HbA1c level is
506 corrected for non-insulin diabetic medication (+ 10.929) and insulin drugs (+ 1.3 x 10.929)[49].
507 The respective changes for individuals who are taking the medication are in the parentheses after
508 each trait; s.d. is the standard deviation computed in the entire population. We verified that the
509 correlation between the corrected quantitative traits and corresponding binary traits is higher
510 compared to the correlation between uncorrected quantitative traits and the same set of binary
511 traits. $\rho(LDL, hypercholesterolemia)$: 0.188 post-medication correction vs -0.005 pre-
512 correction. $\rho(Systolic\ blood\ pressure, hypertension)$: 0.519 post-medication correction vs
513 0.425 pre-correction. $\rho(HbA1c, T2D)$: 0.565 post-medication correction vs 0.524 pre-correction.
514 Both corrected and uncorrected values were included in the final 36 quantitative traits.
515
516 In our analyses, smoking status is defined as an ordinal variable with the following values: never
517 (0), previous (1), current (2) (**Supplementary Table 4**).
518
519 To select quantitative traits that are most relevant to the nine diseases, we further computed the
520 correlation between the 36 quantitative traits and the nine disease traits and selected 16 of the 36
521 quantitative traits based on liability-scale correlation [33]; the included quantitative traits are
522 among the top 3 correlated traits for at least one of the nine binary diseases.
523
524 Heritability and genetic correlation
525 We estimated heritability using the REML function of BOLT-LMM[19] version 2.4.1. 180,026
526 individuals were divided into 5 age bins based on the baseline visit age. We performed REML
527 analysis for each age bin using sex and baseline visit age as covariates; we use the same 536,492
528 HapMap3 SNPs that have moderate LD with each other which is the same as the PRS section,
529 see below. We also computed the heritability of 16 quantitative traits and nine diseases in the
530 entire population.
531

532 We estimated genetic correlation between age bins for the 16 quantitative traits using LDscore
533 regression[50]. First, we used the mixed-effect model to compute summary statistics for each age
534 bin using BOLT-LMM version 2.4.1. We used the same set of variants and individuals as the
535 heritability estimation. Since BOLT-LMM is a mixed effect model that controls population
536 stratification, we constrained the heritability intercept of LDSC to 1.0; we constrained covariance
537 intercept to be 0 as there is no sample overlap between different age bins. We run cross-trait
538 LDSC for each age-bin pair (10 pairs in total for 5 age bins) to estimate the genetic correlation
539 and its standard error.
540
541 Testing for heritability changes across age bins
542 We tested the age-dependency of heritability using heritability estimates with standard error
543 across the five age bins. We used likelihood ratio tests to identify non-constant heritability across
544 age bins. We tested two nested models: $H_0: h^2 \sim N(0 \times age + b, s.e.(h^2))$ and
545 $H_1: h^2 \sim N(a \times age + b, s.e.(h^2))$. We estimated b under H_0 and a, b under H_1 using
546 maximum likelihood estimators across the five heritability estimates. For each age quintile, we
547 use the median age to fit the model. The slope a estimated under H_1 are the per year change of
548 h^2. We use Monte-Carlo sampling of h^2 for each age quintile from a Gaussian distribution with
549 mean equals to the point estimates and variance equals to s.e.. We estimate a, b of each Monte-
550 Carlo sample. The s.d. of a estimates across Monte-Carlo samples are the s.e. of the estimates.
551 We note this approach relies on the fact that samples are non overlapping across age quintiles.
552
553 In all analyses, we report the relative change of heritability compared to the heritability estimate
554 in the entire population.
555
556 Testing for genetic correlation less than 1 between age bins
557 The quantity of interest is the difference between genetic correlation and 1: $1 - \rho_g$. First, we
558 scale genetic correlation using $\rho_{normalised} = exp(10 \times ln\, \rho_{\Delta age} / \Delta age)$ to account for the
559 varying age differences of age-bin pairs; the age differences are computed using the median of
560 each age quintile. Scaling on the exponential scale aligns with a Wiener process of liability w.r.t
561 age (see below). For 5 age bins, we can estimate 10 genetic correlations between pairs of age
562 bins; these 10 genetic correlations have four degrees of freedom. Therefore, we use inverse-
563 variance weighting to meta-analyse four of the 10 scaled ρ_g (we use ρ_g of neighboring age-bin
564 pairs 1-2, 2-3, 3-4, and 4-5) to compute one 10-year r_g for each trait; standard errors of the 10-
565 year r_g estimates are used for inverse-variance weights.
566
567 Computing phenotypic correlation across age points
568 Under the assumption that random variance accumulates linearly w.r.t. age (as in a Wiener
569 process), the correlation between liability across age bins is a function on the multiplicity scale
570 $\rho_{\Delta age} = e^{-\beta\, \Delta age}$. Therefore, we computed the expected 10-year genetic and phenotypic

correlation by $exp(10 \times ln\, \rho_{\Delta age} / \Delta age)$ to make the correlations comparable for age bin pairs with different age differences. We computed phenotype correlations across individuals who have three visits to the UK Biobank. We remove the impact of measurement error by computing a ratio of two correlations $\rho_{\Delta age} = \rho_l(t_1, t_3)/\rho_l\,(t_1, t_2)$, which cancels out the measurement error, and we use the average age difference between second and third visit ($\Delta age = t_3 - t_2$) to scale the estimate.

Testing the impact of selection in recruitment process

To test for whether the age-dependent heritability changes can be attributed to selected recruitment of healthier individuals at older age groups[21], we computed the number of past diagnosis records as an indicator of health status and created samples with matched age but different past diagnosis. We used health records from both GP and HES, and divided the target population into two groups, "healthy" versus "unhealthy", using the median number of prevalent records (median=16). We then use inverse probability weights to sample 45,267 individuals from both groups, resulting in two samples that have matched age distributions (mean: 55.9 vs. 56.6, respectively) but different numbers of past diseases (mean: 6.8 vs 34.6, respectively); in comparison, top and bottom age quintile has an average age of 67.5 and 45.3 and an average of 24.2 and 18.7 of past diseases, respectively. We compute heritability of the 16 quantitative for both groups using the same procedure as for age quintiles.

PRS construction

We obtained 536,492 HapMap3 SNPs using pruning parameters of window size=50 kb, step size=5 kb, and r^2 threshold=0.8; selection of SNPs makes mixed effect model computational tractable. We then used BOLT-LMM to estimate PRS, using genetic sex and age at baseline as covariates, using 5-fold cross validation for the 9 diseases and 16 quantitative traits. PRS are scaled to have mean=0 and sd=1 in the entire population.

PRS incident case prediction and prevalent case association

For incident case prediction, we first divided cases into five age quintiles based on their first age-at-diagnosis; for each age quintile, we define case control status based using interval-censor procedure [8], where cases are defined as those who are diagnosed within the age interval and controls are defined as those who remained healthy till the end of age interval or lost to follow up within the age interval. We then down sampled the controls for each age bin to have the same number as the cases. As a result, for a given disease, each age interval has exactly the same number of cases and controls which ensures the odds ratio and hazard ratio are comparable across each age bin. When evaluating PRS using linear, logistic, and Cox regression models, we included genetic sex and top five genetic PCs as covariates. When evaluating PRS using observed-scale R^2, we first regress the outcome on genetic sex and top five genetic PCs, then compute Pearson's correlation between the residual and PRS; the square of Pearson's correlation is the observed-scale R^2 with 1:1 case control ratio.

611
612 For prevalent cases association, we used the five median case age of the respective age intervals
613 as the baseline age points and considered all individuals who have been followed up past the
614 baseline age point. The prevalence cases are defined as those who have at least one diagnosis
615 record before the baseline age point. We sampled controls to be the same number as cases for
616 each age point, so that for a given disease, the effect sizes of linear, logistic, and Cox regression
617 across five baseline age points are comparable. The regression models and observed-scale R^2
618 were computed using the same covariates as in incident case association.
619
620 Estimated disease liability
621 We use 36 continuous traits measured at baseline to predict the 9 binary disease traits; the
622 resulting predictor is the *estimated disease liability*. Cases are defined as the union of both
623 incident and prevalent disease. We use LASSO linear model (instead of logistic regression as we
624 assume a liability-threshold model) to train the prediction models with 10-fold cross validation;
625 the regularization coefficients are chosen by the cross-validation with both 1se (default setting of
626 the R glmnet package[51,52]) and 2se (stronger regularization). We chose the predicted liability
627 using the 2se model as it has a similar liability-scale correlation (average=0.60 across 9 diseases)
628 with the binary trait to the 1se model (average=0.61 across 9 diseases), while being more
629 explainable and less susceptible to overfitting. The models were fitted in the entire population
630 without including age as a covariate so that the predicted disease liability represents the
631 approximate disease liability at the age of baseline visit.
632
633 We used the same procedure as the quantitative traits analysis to estimate heritability and genetic
634 correlation for predicted liability. We used BOLT-REML to estimate heritability. We used
635 BOLT-LMM to compute GWAS summary statistics then use cross-trait LDSC to estimate
636 genetic correlation of each age-bin pair (10 pairs in total for 5 age bins) to estimate the genetic
637 correlation and its standard error. We did not constrain intercepts for cross-trait LDSC to avoid
638 potential bias population relatedness.
639
640 Simulation of linear liability-threshold model
641 We simulated genetic variance G and environment variance E from normal distribution with
642 mean 0 and variance equal to h^2 and $(1-h^2)$ respectively. Liability L equals the sum of G and E
643 for each individual. To simulate liability increasing with age, we take 2% of the simulated
644 individuals with the highest liability as the youngest disease group, top 2-4% of liability as the
645 second age group and repeated the procedure to obtain five groups of individuals with increasing
646 onset age. Each disease threshold corresponds to the disease cut off at an age point. Prevalent
647 cases are defined as the individuals that have liabilities higher than the threshold at a specific age
648 point; incident cases are defined as individuals in the bin near the liability threshold at a specific
649 age point (i.e. all individuals with liability near the corresponding liability); controls are defined
650 as all individuals excluding prevalent cases (i.e. all individuals have liability lower than the

651 corresponding liability).We simulated 100,000 individuals, with h^2=0.3 and using five age bins
652 of 2% of individuals, which matches the disease prevalence and sample size in empirical
653 analyses.
654
655 We note our simulation uses percentiles of individuals to represent cases with increasing age,
656 which aligns with the empirical analysis (see below) where we divided cases into quintiles based
657 on the diagnosis age. We note under the proportional amplifciation model, the liability percentile
658 of each individual does not change, which means this model is invariant to proportional
659 amplification.
660
661 Simulation of EA liability-threshold model
662 We simulated initial liability L using the same procedure as the linear liability-threshold model.
663 For each age bin, we sample cumulative environmental variance E_a from normal distribution
664 with 0 mean and 0.05 variance. We then cumulatively add these sampled environmental
665 variances to the liability when moving to an older age quintile, which will result in 20% more
666 accumulated variance in the fifth age quintile. In empirical data, we found ~20% decrease in
667 heritability over 20 years for quantitative traits, which motivates our choice of simulation
668 parameters.
669
670 We defined prevalent cases as individuals who have got disease at any prior age bin or the
671 current age bin, and incident cases as those who get disease within the current age bin. For each
672 age bin, we take the top 2% individuals who have not prevalent diseases to simulate that liability
673 increases with age. We note this simulation procedure makes the number of cases equal to
674 previous simulation of the linear model so the metrics in **Figure 4B** are comparable.
675
676 Estimating age-dependent prediction accuracy under the linear liability-threshold model
677 We use rank normal transformation of estimated liability to create a *quantitative risk score*
678 *(QRS)*. QRS combines both G and E information which is different from PRS that only captures
679 G information; under the linear liability-threshold model, QRS and PRS has the sample age-
680 dependent prediction accuracy profile when their liability-scale R^2 are equivalent across the
681 population (**Figure 4C**). We performed the following 6 steps to use QRS to estimate expected
682 age-dependency of PRS under the liability-threshold model. (1) QRS are rank normal
683 transformed to have similar distributions as PRS. (2) QRS are adjusted for age at measurement
684 and genetic sex; PRS are adjusted for first 5 genetic PCs and genetic sex. Adjustment of
685 covariates ensures QRS and PRS are comparable under the linear liability-threshold model for
686 each age bin, as QRS will change with age while PRS does not change with age. (3) We
687 computed the liability-scale R^2 of QRS and PRS using all individuals with primary care
688 information (N = 215,162); cases are defined as the union of prevalent cases and incident cases.
689 We computed observed-scale R^2 for both QRS and PRS and transformed observed-scale R^2 to
690 liability-scale R^2 using equation 14 of ref [33]. (4) We added gaussian noise (mean = 0) to QRS so

691 that the new QRS has the same liability-scale R^2 as PRS. (5) We computed QRS observed-scale
692 R^2 for each age bin using the same case-control definition as incident case prediction of PRS. We
693 note a caveat that some QRS are measured after disease diagnosis. Our choice is based on two
694 reasons: first, under the linear liability-threshold model, QRS (age and sex adjusted) represents
695 the liability that remains constant across age; second, observed-scale R^2 for QRS and PRS are
696 computed using the same samples, making them comparable. We use QRS to predict incident
697 cases at baseline visit and found similar results, see sections pertains to "non-genetic predictors".
698 (6) We performed Monte-Carlo sampling to account for two sources of uncertainty: (i) the
699 process to add noise to QRS and (ii) control sampling within each age bin. We reported mean
700 and standard deviation of 50 Monte-Carlo sampling estimates for each parameter.
701
702 We define the proportion of observed decrease in PRS accuracy explained by each model as:
703 $$\tau = \sum_{diseases} \max(\Delta R^2_{QRS}, \Delta R^2_{PRS}) / \sum_{diseases} \Delta R^2_{PRS}.$$
704 The max in the numerator reflects the constraint that the proportion of age-dependent PRS
705 accuracy that can be explained is less than 100%. Therefore, diseases with more decrease in QRS
706 accuracy than PRS accuracy are assigned the same value in numerator and denominator. This
707 choice is justified by empirical data as we do not observe significantly more decrease in QRS
708 accuracy than PRS accuracy at a nominal *p*-value of 0.05, except for CAD.
709
710 <u>Estimating age-dependent prediction accuracy under the EA + liability-threshold model</u>
711 We multiplied the estimated slope from QRS with the slope of h^2 of predicted liability to
712 estimate the expected decrease under the EA + liability-threshold model. Under the EA model
713 PRS prediction accuracy is proportional to h^2 of disease liability at each age point. The EA +
714 liability-threshold model estimates capture both the age-dependency from the linear liability-
715 threshold model (captured by QRS) and the EA model (captured by the Δh^2 of predicted
716 liability). The expected change is computed as 1 - (1 + $\Delta R^2{}_{QRS}$) ×(1 + $\Delta h^2{}_{predicted-liability}$).
717 We use Monte-Carlo sampling of $\Delta R^2{}_{QRS}$ and $\Delta h^2{}_{predicted-liability}$ to estimate the standard
718 error of the estimator; we omit the sampling covariance between $\Delta R^2{}_{QRS}$ and
719 $\Delta h^2{}_{predicted-liability}$ as they were estimated from approximately independent information (*i.e.*
720 $\Delta R^2{}_{QRS}$ were estimated using age quintiles of cases and baseline measurements, while
721 $\Delta h^2{}_{predicted-liability}$ uses genetic information).
722
723 <u>Incident case prediction with non-genetic predictors</u>
724 For environment variable predictors, we divided incident cases into five age bins using the age at
725 first diagnosis visit. We note that in contrast to PRS prediction accuracy, we excluded
726 individuals who have prevalent cases before baseline visits as environment variables are
727 measured at baseline visit. The definition of incident cases and controls for each age quintile,
728 down sampling of control is the same as the PRS incident case prediction. We computed
729 observed-scale R^2 for each environment predictor by regression of sex and top five genetic PCs

from the outcomes and computed Pearson's correlation between the outcome residual and the predictor; the square of Pearson's correlation is the observed-scale R^2 with 1:1 case control ratio.

We analyzed 10 predictors including 9 environment predictors and PRS. We computed the relative change of observed-scale R^2 compared to the observed-scale R^2 estimate in the entire population. Observed-scale R^2 in the entire population were transformed to liability-scale R^2 using equation 14 of ref [33]. When computing the relationship between liability-scale R^2 (in the entire population) to the change of observed-scale R^2, we only include 61 of 90 predictors that have liability-scale R^2 larger than 5% to ensure there is sufficient power to detect age-dependency.

Code Availability

Code to replicate all analyses in the manuscript is available at https://github.com/Xilin-Jiang/GxAge

Data Availability

Summary data in the manuscript is available at https://github.com/Xilin-Jiang/GxAge

Acknowledgements

Use of the UK Biobank data was performed under application number 7439. This research was funded by Wellcome Trust early-career award 227566/Z/23/Z (X.J.) and the National Institute Of General Medical Sciences of the National Institutes of Health under Award Number R35GM16046 (A.D.). M.I. is supported by the Munz Chair of Cardiovascular Prediction and Prevention and the NIHR Cambridge Biomedical Research Centre (NIHR203312) as well as by the UK Economic and Social Research 878 Council (ES/T013192/1). J.D. is supported by a British Heart Foundation Personal Chair. This work was supported by core funding from the British Heart Foundation (RG/F/23/110103), NIHR Cambridge Biomedical Research Centre (NIHR203312), BHF Chair Award (CH/12/2/29428), Cambridge BHF Centre of Research Excellence (RE/24/130011) and by Health Data Research UK, which is funded by the UK Medical Research Council, Engineering and Physical Sciences Research Council, Economic and Social Research Council, Department of Health and Social Care (England), Chief Scientist Office of the Scottish Government Health and Social Care Directorates, Health and Social Care Research and Development Division (Welsh Government), Public Health Agency (Northern Ireland), British Heart Foundation and the Wellcome Trust. The views expressed are those of the authors and not necessarily those of the NIHR, the Department of Health and Social Care, or the National Institutes of Health.

Declaration of interests

G.M. is a shareholder in Genomics PLC and a partner in Peptide Groove LLP. G.L. is a shareholder in Genomics PLC. M.I. is a trustee of the Public Health Genomics (PHG) Foundation, a member of the Scientific Advisory Board of Open Targets, and has research

collaborations with AstraZeneca, Nightingale Health and Pfizer which are unrelated to this study.

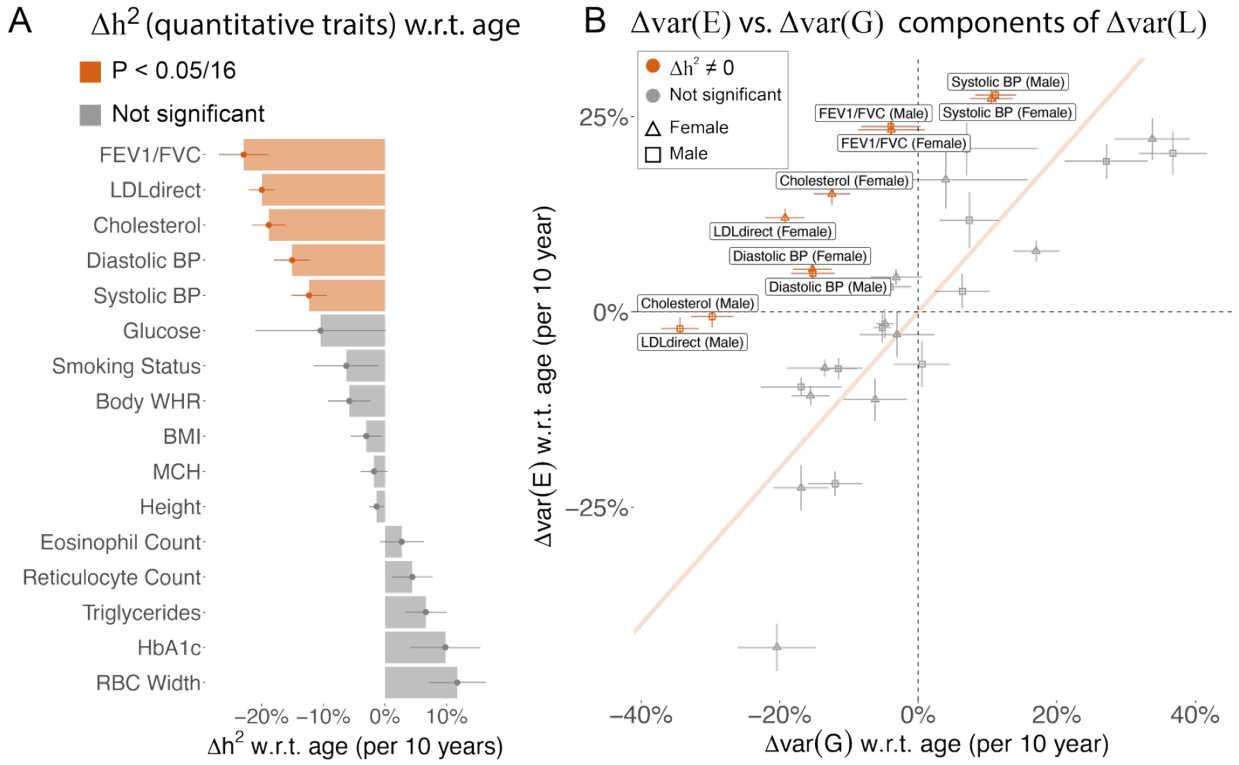

Figure 1. Age-dependent variance of quantitative traits. (A) Heritability changes per 10-years for 16 quantitative traits. Red bars show significant heritability changes across age; error bars show standard error via Monte-Carlo sampling. (B) 10-year change for genetic and environment variance for the 16 quantitative traits. Traits with significant age-dependent heritability are highlighted in red. Traits in grey show evidence of proportional amplification of genetic and environmental variance. Error bars are standard error via Monte-Carlo sampling. Numerical results are provided in **Supplementary Table 5 and Supplementary Table 7**. We note that no estimates are significantly outside the plausible range and that allowing estimates outside of the plausible range is necessary to ensure unbiasedness of estimates.

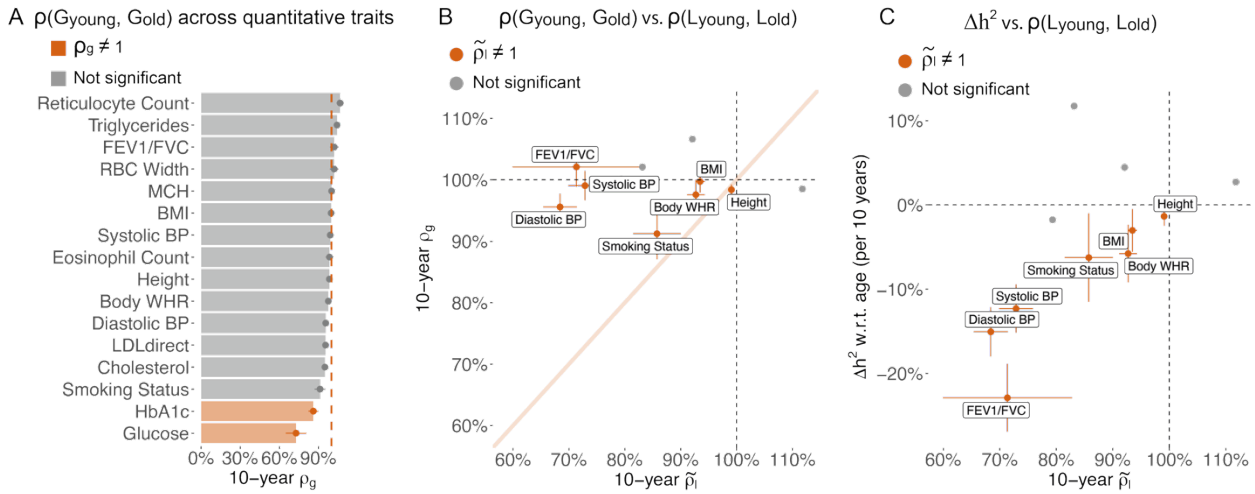

Figure 2. Genetic liability is more correlated across young and older age groups than environmental liability. (A) 10-year genetic correlation between younger and older age bins for 16 quantitative traits. We report the genetic correlation per 10-year age difference. (B) Scatter plot of 10-year genetic correlation versus denoised 10-year phenotypic correlation for the 11 quantitative traits that have three measurements per individual. We found no genetic correlation or phenotypic correlation that are significantly higher than 1 at nominal *p*-value = 0.05. (C) Scatter plot of heritability changes per 10-years versus denoised 10-year phenotypic correlation for the 11 quantitative traits that have three measurements per individual. Traits with denoised 10-year phenotypic correlation significantly different from 1 are shown in red and labeled in panel B and C; non-significant traits are shown in grey. Error bars for phenotypic correlation are standard error via bootstrapping over individuals; error bars for genetic correlation are standard error after meta-analysis across 4 age-bin pairs. Numerical results are provided in **Supplementary Table 8-9**. We note that no estimates are significantly outside the plausible range and that allowing estimates outside of the plausible range is necessary to ensure unbiasedness of estimates.

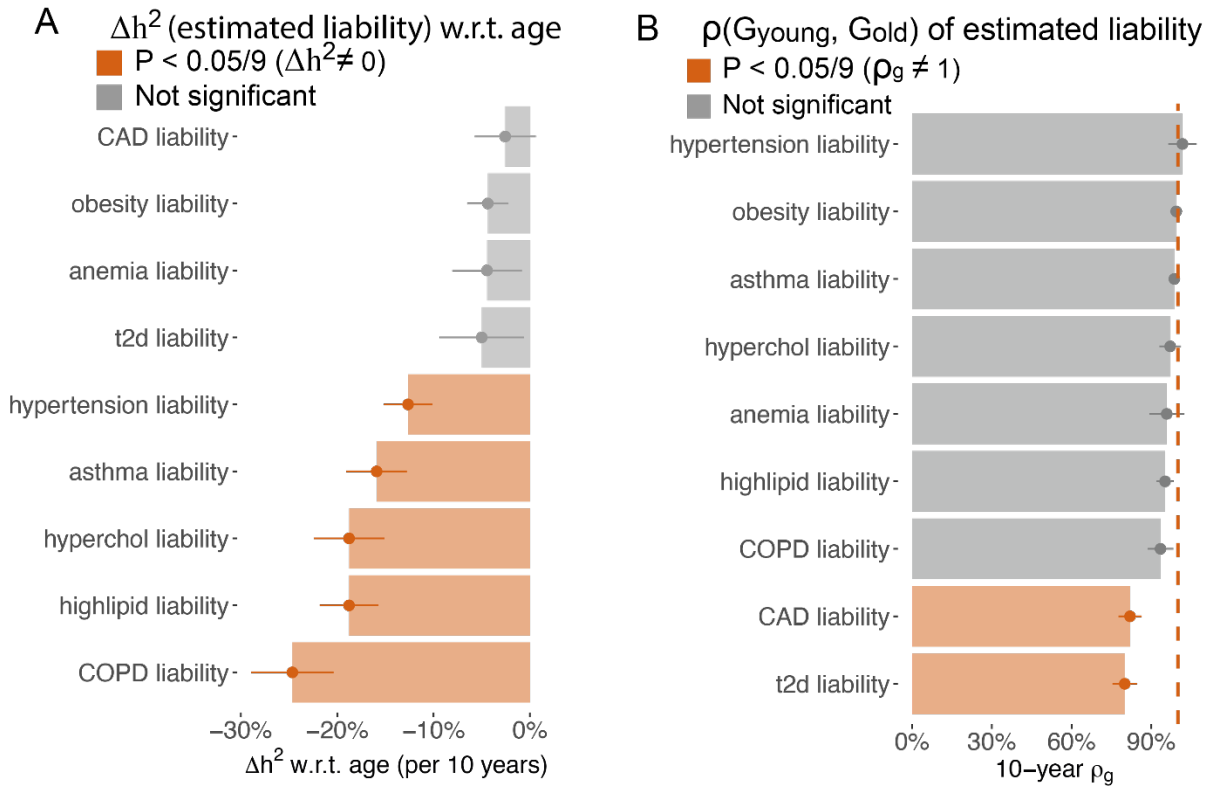

Figure 3. Age-dependent genetic architecture of estimated liability supports the EA model. (A) 10-year heritability change for estimated liability of 9 diseases; error bars show standard error via Monte-Carlo sampling. (B) 10-year genetic correlation for the estimated liability of 9 diseases. Error bars are standard error via meta-analysis of 10 age bin pairs. Numerical results are provided in **Supplementary Table 11-12**.

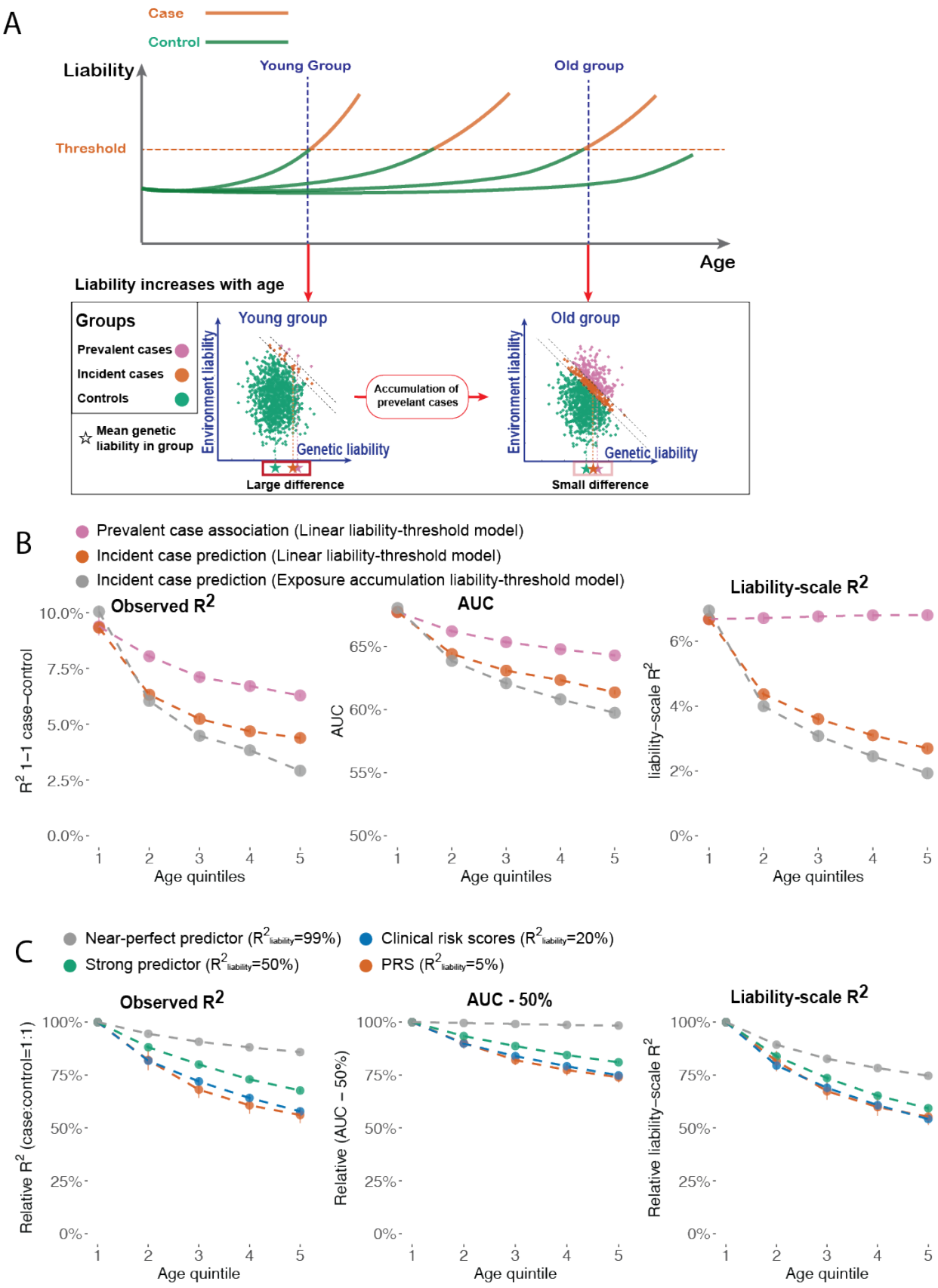
A
Case
Control
Liability
Young Group
Old group
Threshold
Age
Liability increases with age
Groups
Prevalent cases
Incident cases
Controls
Mean genetic liability in group
Young group
Old group
Environment liability
Genetic liability
Accumulation of prevelant cases
Large difference
Small difference
B
Prevalent case association (Linear liability-threshold model)
Incident case prediction (Linear liability-threshold model)
Incident case prediction (Exposure accumulation liability-threshold model)
Observed R2
AUC
Liability-scale R2
R2 1–1 case–control
liability–scale R2
Age quintiles
C
Near-perfect predictor (R2liability=99%)
Strong predictor (R2liability=50%)
Clinical risk scores (R2liability=20%)
PRS (R2liability=5%)
Observed R2
AUC - 50%
Liability-scale R2
Relative R2 (case:control=1:1)
Relative (AUC – 50%)
Relative liability–scale R2
Age quintile

815

Figure 4. Liability-threshold model and the EA model explains age-dependent disease prediction accuracy in simulations. (A) Schematic figure explaining the decreasing disease prediction accuracy with age. In the top panel, each line represents the liability trajectory of an individual. The panel below shows the joint distribution of genetic and environmental liability at two age points. At later age points, cases are more similar to controls compared to earlier age points. (B) Prevalent case association accuracy (purple), incident case prediction accuracy (red), and Incident case prediction under the EA model (grey) across different age quintiles of cases. Prediction accuracy is measured by observed-scale R^2 in 1:1 case-control matched samples, AUC, and liability scale R^2 (C) Incident case prediction accuracy of predictors with different liability-scale R^2.

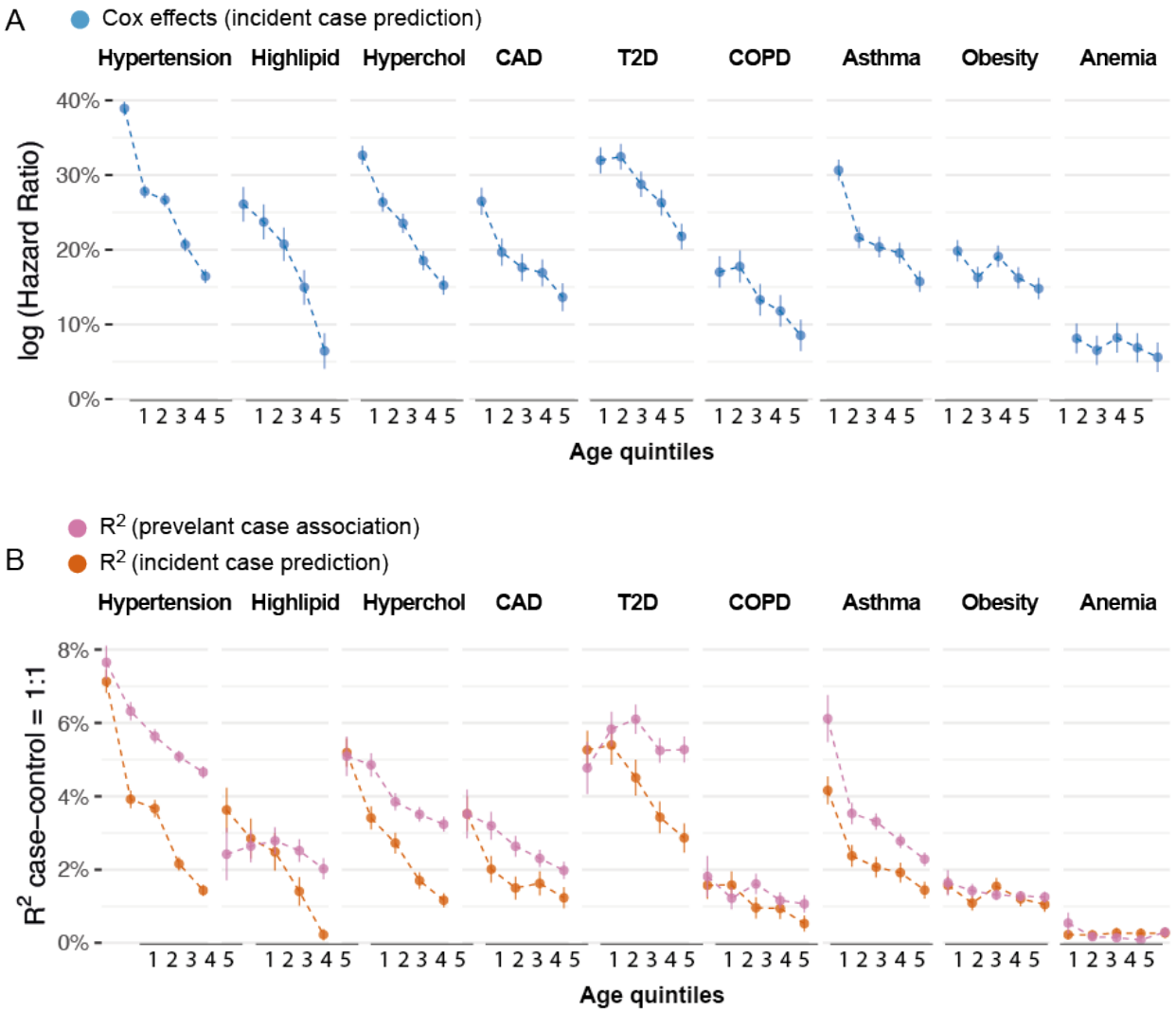

Figure 5: Age-dependent incident case prediction accuracy in 9 diseases. (A) Cox log hazard ratio of PRS on 9 diseases across 5 age quintiles. Each age bin has the same number of cases and 1:1 case-control ratio. Bars show standard error. (B) Age-dependent incident case prediction compared to prevalent case association accuracy in 9 diseases. Numerical results are provided in **Supplementary Table 13-14**.

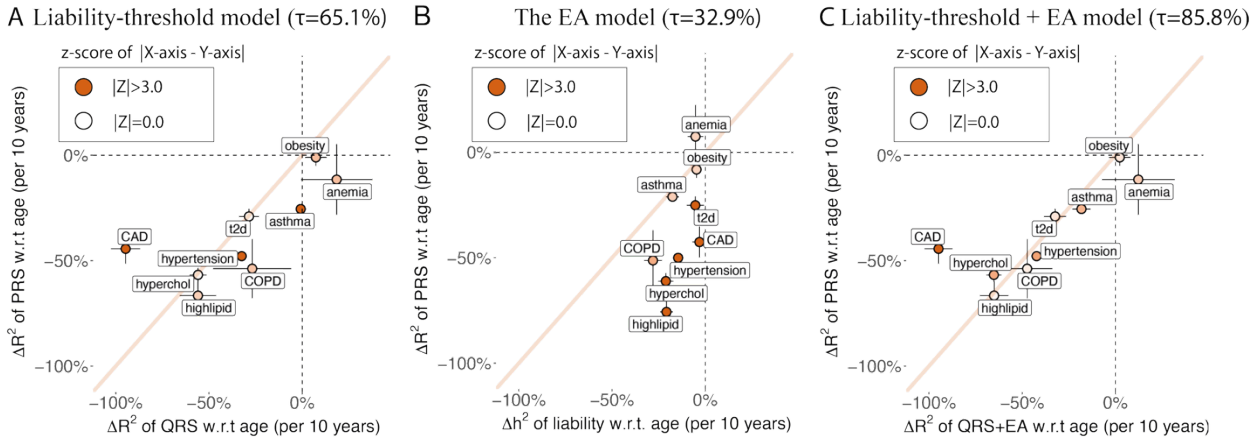

Figure 6: Liability-threshold model and the EA model explain age-dependent PRS prediction accuracy. (A) 10-year change in QRS prediction R^2 under the liability-threshold model versus 10-year change in PRS prediction R^2 for 9 disease traits. (B) 10-year heritability change in estimated disease liability versus 10-year change in PRS prediction R^2 for corresponding disease traits. (C) 10-year change in QRS prediction R^2 under the liability-threshold+EA model versus 10-year change in PRS prediction R^2 for 9 disease traits. Diagonal line has slope equals to 1. Bars show the se and color shows the z-score of difference in X and Y values of each dot. τ is the proportion of observed decrease in PRS accuracy explained by each model (**Methods**). Numerical results are provided in **Supplementary Table 15-17**. We note that no estimates are significantly outside the plausible range and that allowing estimates outside of the plausible range is necessary to ensure unbiasedness of estimates.

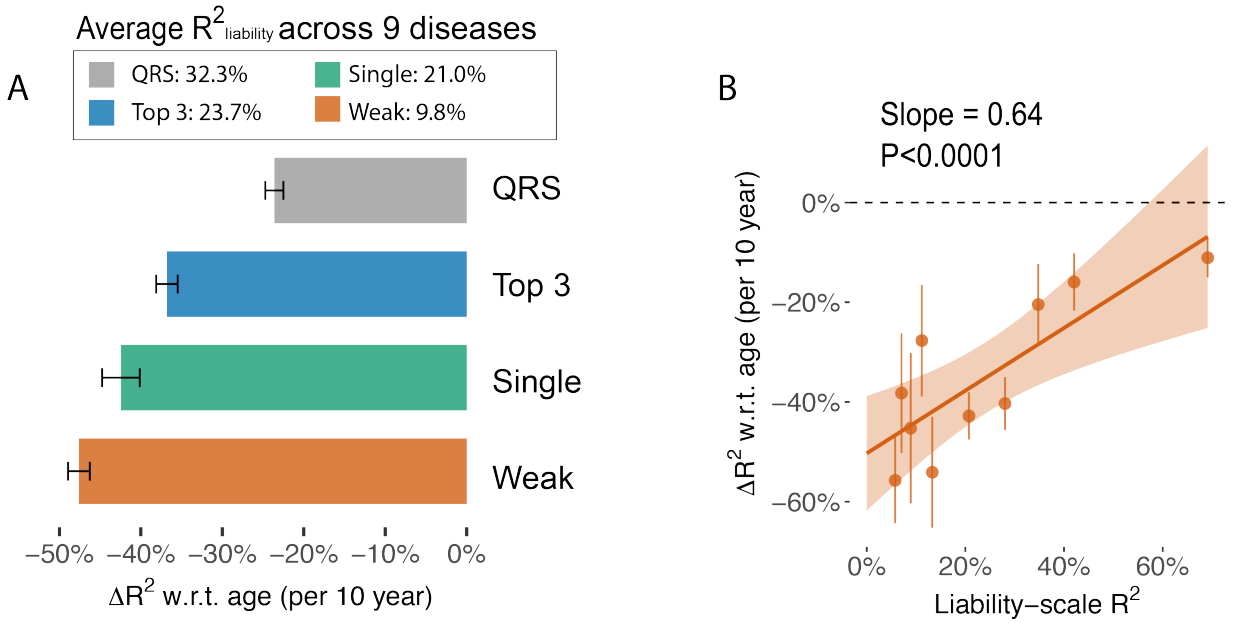

Figure 7. Risk models with higher liability-scale R^2 are less attenuated when predicting late-onset diseases. (A) Age-dependent prediction accuracy of predictors averaged across 9 diseases. X-axis shows the per-10-year change of prediction R^2 computed in 1-1 case control matching groups. QRS: predicted liability using 36 quantitative traits. Top 3: linear predictors use the top three quantitative traits that have the highest correlation with the diseases. Single (Strong): using a single quantitative trait to predict incident diseases, averaged across the top three traits as in the "Top 3" group; Single (Weak): the average between 4th and 5th predictor of each disease. (B) Scatter plot comparing the liability-scale R^2 (without age stratification) with the change of R^2 w.r.t. age across predictor-disease pairs. Predictor-disease pairs are grouped into 10 deciles based on liability-scale R^2 for visualization. The red line shows a regression line with confidence interval. Numerical results are provided in **Supplementary Table 18-19**.

862
863
864 **References:**

865 1. Kroemer, G. *et al.* From geroscience to precision geromedicine: Understanding and
866 managing aging. *Cell* **188**, 2043–2062 (2025).
867 2. Moqri, M. *et al.* Biomarkers of aging for the identification and evaluation of longevity
868 interventions. *Cell* **186**, 3758–3775 (2023).
869 3. Simino, J. *et al.* Gene-age interactions in blood pressure regulation: a large-scale
870 investigation with the CHARGE, Global BPgen, and ICBP Consortia. *Am. J. Hum. Genet.*
871 **95**, 24–38 (2014).
872 4. Robinson, M. R. *et al.* Genotype-covariate interaction effects and the heritability of adult
873 body mass index. *Nat. Genet.* **49**, 1174–1181 (2017).
874 5. Winkler, T. W. *et al.* Genetic-by-age interaction analyses on complex traits in UK Biobank
875 and their potential to identify effects on longitudinal trait change. *Genome Biol.* **25**, 300
876 (2024).
877 6. Miao, J. *et al.* PIGEON: a statistical framework for estimating gene-environment interaction
878 for polygenic traits. *Nat. Hum. Behav.* 1–15 (2025).
879 7. Zhu, C. *et al.* Amplification is the primary mode of gene-by-sex interaction in complex
880 human traits. *Cell Genomics* **3**, (2023).
881 8. Jiang, X., Holmes, C. & McVean, G. The impact of age on genetic risk for common
882 diseases. *PLoS Genet.* **17**, e1009723 (2021).
883 9. Sakaue, S. *et al.* Trans-biobank analysis with 676,000 individuals elucidates the association
884 of polygenic risk scores of complex traits with human lifespan. *Nat. Med.* **26**, 542–548
885 (2020).

886 10. Jukarainen, S. *et al.* Genetic risk factors have a substantial impact on healthy life years. *Nat.*
887 *Med.* **28**, 1893–1901 (2022).
888 11. Dahl, A. *et al.* A Robust Method Uncovers Significant Context-Specific Heritability in
889 Diverse Complex Traits. *Am. J. Hum. Genet.* **106**, 71–91 (2020).
890 12. Pazokitoroudi, A. *et al.* A scalable and robust variance components method reveals insights
891 into the architecture of gene-environment interactions underlying complex traits. *Am. J.*
892 *Hum. Genet.* **111**, 1462–1480 (2024).
893 13. Thompson, D. J. *et al.* A systematic evaluation of the performance and properties of the UK
894 Biobank Polygenic Risk Score (PRS) Release. *PLoS One* **19**, e0307270 (2024).
895 14. Argentieri, M. A. *et al.* Integrating the environmental and genetic architectures of aging and
896 mortality. *Nat. Med.* **31**, 1016–1025 (2025).
897 15. Durvasula, A. & Price, A. L. Distinct explanations underlie gene-environment interactions
898 in the UK Biobank. *Am. J. Hum. Genet.* **112**, 644–658 (2025).
899 16. Zaitlen, N. *et al.* Informed conditioning on clinical covariates increases power in case-
900 control association studies. *PLoS Genet.* **8**, e1003032 (2012).
901 17. Pedersen, E. M. *et al.* Accounting for age of onset and family history improves power in
902 genome-wide association studies. *Am. J. Hum. Genet.* **109**, 417–432 (2022).
903 18. Aschard, H., Zaitlen, N., Lindström, S. & Kraft, P. Variation in predictive ability of
904 common genetic variants by established strata: the example of breast cancer and age.
905 *Epidemiology* **26**, 51–58 (2015).
906 19. Loh, P.-R. *et al.* Efficient Bayesian mixed-model analysis increases association power in
907 large cohorts. *Nat. Genet.* **47**, 284–290 (2015).

908 20. Weissbrod, O. *et al.* Leveraging fine-mapping and multipopulation training data to improve
909 cross-population polygenic risk scores. *Nat. Genet.* **54**, 450–458 (2022).
910 21. Fry, A. *et al.* Comparison of sociodemographic and health-related characteristics of UK
911 Biobank participants with those of the general population. *Am. J. Epidemiol.* **186**, 1026–
912 1034 (2017).
913 22. Tibshirani, R. Regression shrinkage and selection via the lasso. *Journal of the royal*
914 *statistical society series b-methodological* **58**, 267–288 (1996).
915 23. Udler, M. S. *et al.* Type 2 diabetes genetic loci informed by multi-trait associations point to
916 disease mechanisms and subtypes: A soft clustering analysis. *PLoS Med.* **15**, e1002654
917 (2018).
918 24. Jiang, X. *et al.* Age-dependent topic modeling of comorbidities in UK Biobank identifies
919 disease subtypes with differential genetic risk. *Nat. Genet.* **55**, 1854–1865 (2023).
920 25. Suzuki, K. *et al.* Genetic drivers of heterogeneity in type 2 diabetes pathophysiology.
921 *Nature* 1–11 (2024).
922 26. Celentano, D. D., Szklo, M. & Farag, Y. *Gordis Epidemiology*. (Elsevier - Health Sciences
923 Division, Philadelphia, PA, 2024).
924 27. Khera, A. V. *et al.* Genome-wide polygenic scores for common diseases identify individuals
925 with risk equivalent to monogenic mutations. *Nat. Genet.* **50**, 1219–1224 (2018).
926 28. Ge, T., Chen, C.-Y., Ni, Y., Feng, Y.-C. A. & Smoller, J. W. Polygenic prediction via
927 Bayesian regression and continuous shrinkage priors. *Nat. Commun.* **10**, 1776 (2019).
928 29. Privé, F., Arbel, J. & Vilhjálmsson, B. J. LDpred2: better, faster, stronger. *Bioinformatics*
929 **36**, 5424–5431 (2021).

930 30. Zheng, Z. *et al.* Leveraging functional genomic annotations and genome coverage to
931 improve polygenic prediction of complex traits within and between ancestries. *Nat. Genet.*
932 **56**, 767–777 (2024).
933 31. SCORE2 working group and ESC Cardiovascular risk collaboration. SCORE2 risk
934 prediction algorithms: new models to estimate 10-year risk of cardiovascular disease in
935 Europe. *Eur. Heart J.* **42**, 2439–2454 (2021).
936 32. Patel, A. P. *et al.* A multi-ancestry polygenic risk score improves risk prediction for
937 coronary artery disease. *Nat. Med.* **29**, 1793–1803 (2023).
938 33. Lee, S. H., Goddard, M. E., Wray, N. R. & Visscher, P. M. A better coefficient of
939 determination for genetic profile analysis. *Genet. Epidemiol.* **36**, 214–224 (2012).
940 34. Chatterjee, N., Shi, J. & García-Closas, M. Developing and evaluating polygenic risk
941 prediction models for stratified disease prevention. *Nat. Rev. Genet.* **17**, 392–406 (2016).
942 35. Torkamani, A., Wineinger, N. E. & Topol, E. J. The personal and clinical utility of
943 polygenic risk scores. *Nat. Rev. Genet.* **19**, 581–590 (2018).
944 36. Kullo, I. J. *et al.* Polygenic scores in biomedical research. *Nat. Rev. Genet.* **23**, 524–532
945 (2022).
946 37. Kullo, I. J. Promoting equity in polygenic risk assessment through global collaboration. *Nat.*
947 *Genet.* **56**, 1780–1787 (2024).
948 38. Genomic data in the All of Us Research Program. *Nature* 1–7 (2024).
949 39. Dempster, E. R. & Lerner, I. M. Heritability of threshold characters. *Genetics* **35**, 212–236
950 (1950).
951 40. Wray, N. R. & Goddard, M. E. Multi-locus models of genetic risk of disease. *Genome Med.*
952 **2**, 10 (2010).

953 41. Lee, S. H., Wray, N. R., Goddard, M. E. & Visscher, P. M. Estimating missing heritability
954 for disease from genome-wide association studies. *Am. J. Hum. Genet.* **88**, 294–305 (2011).
955 42. Witte, J. S., Visscher, P. M. & Wray, N. R. The contribution of genetic variants to disease
956 depends on the ruler. *Nat. Rev. Genet.* **15**, 765–776 (2014).
957 43. Hujoel, M. L. A., Gazal, S., Loh, P.-R., Patterson, N. & Price, A. L. Liability threshold
958 modeling of case-control status and family history of disease increases association power.
959 *Nat. Genet.* **52**, 541–547 (2020).
960 44. Hujoel, M. L. A., Loh, P.-R., Neale, B. M. & Price, A. L. Incorporating family history of
961 disease improves polygenic risk scores in diverse populations. *Cell Genom.* **2**, 100152
962 (2022).
963 45. Pedersen, E. M. *et al.* ADuLT: An efficient and robust time-to-event GWAS. *Nat. Commun.*
964 **14**, 5553 (2023).
965 46. Wu, P. *et al.* Mapping ICD-10 and ICD-10-CM Codes to Phecodes: Workflow
966 Development and Initial Evaluation. *JMIR Med Inform* **7**, e14325 (2019).
967 47. Kofink, D. *et al.* Statin Effects on Metabolic Profiles: Data From the PREVEND IT
968 (Prevention of Renal and Vascular End-stage Disease Intervention Trial). *Circ. Cardiovasc.*
969 *Genet.* **10**, (2017).
970 48. Wu, J. *et al.* A summary of the effects of antihypertensive medications on measured blood
971 pressure. *Am. J. Hypertens.* **18**, 935–942 (2005).
972 49. Esposito, K., Chiodini, P., Bellastella, G., Maiorino, M. I. & Giugliano, D. Proportion of
973 patients at HbA1c target <7% with eight classes of antidiabetic drugs in type 2 diabetes:
974 systematic review of 218 randomized controlled trials with 78 945 patients. *Diabetes Obes.*
975 *Metab.* **14**, 228–233 (2012).

50. Bulik-Sullivan, B. K. *et al.* LD Score regression distinguishes confounding from polygenicity in genome-wide association studies. *Nat. Genet.* **47**, 291–295 (2015).

51. Friedman, J., Hastie, T. & Tibshirani, R. Regularization paths for generalized linear models via coordinate descent. *J. Stat. Softw.* **33**, 1–22 (2010).

52. Tay, J. K., Narasimhan, B. & Hastie, T. Elastic net regularization paths for all generalized linear models. *J. Stat. Softw.* **106**, 1–31 (2023).